JOURNAL OF NANO- AND ELECTRONIC PHYSICS
Vol. **5** No 3, 03055(7pp) (2013)

ЖУРНАЛ НАНО- ТА ЕЛЕКТРОННОЇ ФІЗИКИ
Том **5** № 3, 03055(7cc) (2013)

Determination of the Nanoparticle Sizes Using AFM Images and Simulation of their Magneto-optical Properties

V.A. Zlenko, M.H. Demydenko, S.I. Protsenko

Sumy State University, 2, Rimsky-Korsakov Str., 40007 Sumy, Ukraine

(Received 10 September 2013; published online 17 October 2013)

This paper describes the geometric models and presents the calculation results of the actual sizes of Ni and Co nanoparticles on the amorphous Si_3N_4/Si substrates obtained by thermal annealing of thin metal films using the data of atomic force microscopy. Results were used in the simulation of magneto-optical properties of arrays of nanoparticles. It is shown that processed by described in the paper equations models allow to obtain a good agreement between calculated and experimentally obtained by MOKE method data.

Keywords: Atomic-force microscopy, Nanoparticle array, MOKE.

PACS numbers: 61.46.Df, 68.37.Lp, 73.61.At, 81.15.Ef

1. INTRODUCTION

Transmission electron microscopy (TEM) as a power tool for the study of the structure and phase composition of nanomaterials allows to estimate geometric dimensions of nano-objects only in the horizontal and vertical planes only at the additional use of the oblique section methods which are not always available. Atomic force microscopy (AFM) is one of a few tools which allows to obtain three-dimensional images of the surface relief of samples and estimate the features of their morphology in the vertical plane. At the same time, AFM method has resolution restrictions that is especially shown in the investigation of nano-objects. From this point of view, geometric parameters of a scanning probe (needle) are one of the most important factors which define both the AFM resolution and image quality.

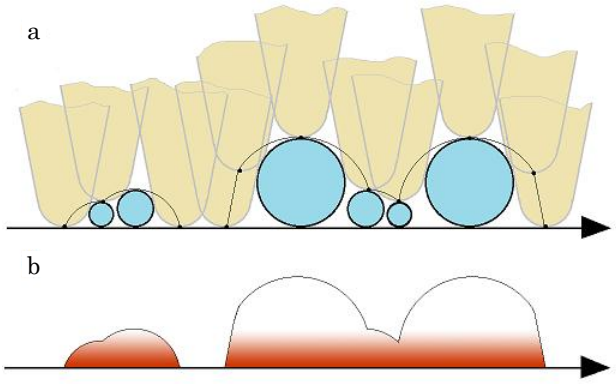

Fig. 1 – Illustration of the mismatch of the real and measured shapes and sizes of objects: a – motion path of scanning probe; b – sample surface relief on the AFM image

As Fig. 1 shows, interpretation of the AFM images becomes more complicated when dimensions of the investigated objects are commensurate with the geometric dimensions of the probe point, and convolution phenomenon introduces an error during measurements of the horizontal (at dense arrangement of objects, vertical as well) dimensions.

2. EXPERIMENTAL TECHNIQUE

Production technique of arrays of Ni and Co nanoparticles (NP) on Si_3N_4/Si amorphous substrates is described in detail in [1, 2] and includes condensation of thin metal layers (effective thickness of 1-3.5 nm) by the thermal evaporation method in the working chamber of vacuum plant VUP-5M (residual gas pressure of 10^{-3} Pa) and their annealing in vacuum. Morphology of NP arrays was investigated using the atomic force microscope Bruker Dimension Edge in semi-contact mode. Magneto-optical properties of NP arrays were studied by using the magneto-optical Kerr effect (MOKE) in the longitudinal measurement geometry. Computer modeling of the magnetic hysteresis curves was performed by the program package oommf [3].

3. CALCULATION TECHNIQUE

Using certain geometric models and calculations [4-6], it is possible to estimate real dimensions by the AFM images with some accuracy. Since two-dimensional arrays of NP on the substrate surface are the object of our investigations, the models described below were used for the interpretation of the AFM images.

In the first case, we will assume in the calculations that needle point has spherical shape, and needle itself has some angle θ at the vertex (Fig. 2a). Investigated objects also have spherical shape, and their diameter D is equal to or less than some boundary calculated diameter ($D_{b.calc}$). In this case, contribution of convolution into particle diameter (horizontal) D_{ex} measured by the AFM image will be defined by the radius of needle point r. The authors of [4] have considered the same model and obtained relation for the calculation of NP diameter D_{calc} by the known AFM needle radius r and particle width on the AFM image D_{ex}:

$$D_{calc} = D_{ex}^2 / 8r\,, \qquad (1)$$

where D_{calc} is the calculated particle radius; D_{ex} is the particle width on the AFM image; r is the radius of AFM needle curvature.

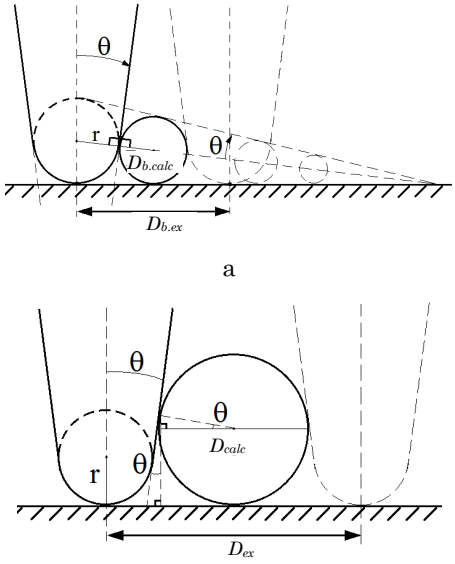

Fig. 2 – Geometric models which describe interaction between AFM probe and spherical particle of different dimensions: a – particle diameter D is less than some boundary diameter $D_{b.nom}$; b – particle diameter is larger than $D_{b.nom}$

However, there are certain restrictions to the use of this model. Analyzing the geometric model represented in Fig. 2b one can conclude that particle radius cannot be larger than some $D_{b.calc}$. The value of $D_{b.calc}$ corresponds to the diameter of sphere inscribed to cone which is clipped by the lower needle point and is the imaginary extension of its shape.

Now we consider the second case (see Fig. 2b). Since particle diameter is larger than $D_{b.calc}$, then not only AFM needle point but also side surface of AFM needle will interact with particle surface. The authors of [5, 6] have solved the problem of the determination of scanning probe radius by the AFM images of spherical objects of the known dimension. We have used the correlations presented by these authors to solve the inverse problem of the calculation of NP dimensions by the known parameters of AFM needle. In this case, one can determine diameter D_{calc} of a spherical object by using the following correlation [5, 6]:

$$D_{nom} = \frac{D_{ex} \cdot \cos\theta}{1+\sin\theta} - 2r \cdot \frac{1-\sin\theta}{1+\sin\theta}, \qquad (2)$$

where θ is the angle at vertex of AFM needle point.

Correlation (2) implies that angle at needle vertex θ will also influence the measured dimensions besides the radius of needle curvature r. In Fig. 3 we illustrate the dependence of the real (calculated) NP diameter D_{calc} on the linear NP dimension (diameter) D_{ex} obtained using AFM in two cases which are described by equations (1) and (2) (radius of AFM needle point r = 10 nm, angle at vertex θ = 15°).

As it is seen from Fig. 3, in the calculations of the real dimensions of a spherical object by the AFM image, transition between the models which are described by equations (1) and (2) should occur in the point of tangency of curves with coordinates ($D_{b.ex}$; $D_{b.calc}$).

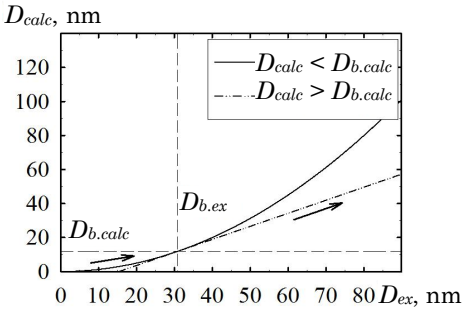

Fig. 3 – Dependence of the NP diameter D_{calc} calculated by two models on the measured diameter D_{ex}

Equating the right sides of equations (1) and (2) and performing the necessary transformations, correlations for the calculation of $D_{b.calc}$ and $D_{b.ex}$ were obtained

$$D_{b.calc} = 2r \cdot \left(\frac{\cos\theta}{1+\sin\theta}\right)^2, \qquad (3)$$

$$D_{b.ex} = 4r\frac{\cos\theta}{1+\sin\theta}. \qquad (4)$$

4. EXPERIMENTAL RESULTS AND DISCUSSION

4.1 Analysis of the surface morphology of arrays of NP

Boundary values of $D_{b.calc}$ and $D_{b.ex}$ calculated by correlations (3) and (4) are equal to 5.93 nm and 30.79 nm, respectively, that illustrates the boundary conditions of the use of correlations in the case of the radius of AFM needle point of r = 10 nm and angle at vertex of θ = 15°.

The above described models and relations were used for the analysis of the AFM images of arrays of Ni and Co NP obtained by the thermal dispersion method on Si_3N_4/Si and Al_2O_3 amorphous substrates. In Fig. 4 we represent the examples of the AFM images of arrays of Ni and Co NP on Si_3N_4/Si substrates obtained by the thermal annealing of thin Ni layers at T_{an} = 990 K and Co layers at T_{an} = 1020 K.

Preliminary treatment of images and determination of the geometric dimensions of NP were carried out by using software Gwyddion 2.26. In Fig. 5a we represent the example of profiles, which are denoted by numerals in Fig. 4b. Measurements were performed on the areas from 0.5 × 0.5 μm to 1 × 1 μm. Modeling and calculation of the data, according to the described models, was carried out by using graphical environment LabVIEW 10.0. Passport data for AFM needle Bruker TESPA was used in the calculations. Angle at needle vertex declared by the manufacturer is θ = 15°, nominal and maximum radiuses of AFM needle point r are equal to 8 and 12 nm, respectively. We should note that in the operation needle always interacts with the sample surface that can lead to both the change in the point shape and increase in its radius. Moreover, as shown in [7], even new needles can have radius of curvature larger than the declared one.

Histograms of NP distribution over horizontal D and vertical h dimensions were built by the measurement results. Example of the obtained dependences is given in Fig. 5b, c.

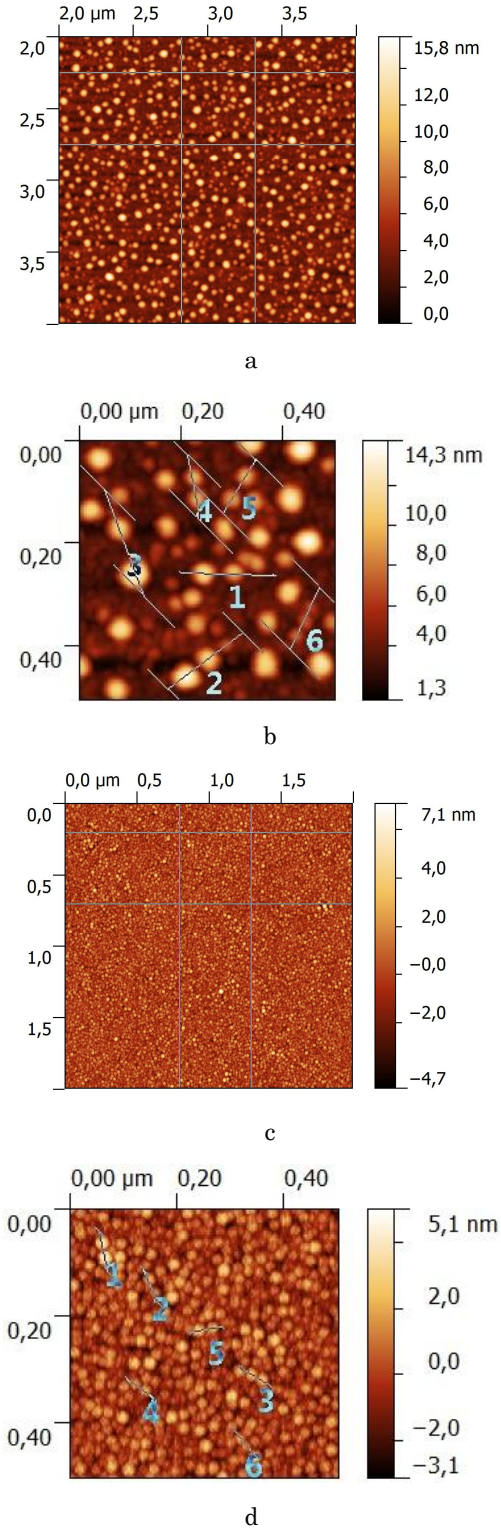

Fig. 4 – AFM images of the arrays of Ni (a) and Co (c) NP on the Si_3N_4/Si substrate (a) and the corresponding increased image areas (b, d)

Calculations of the particle diameter performed for r = 8-12 nm indicate the considerable increase in the NP dimension on the AFM image due to the effect of convolution (see Fig. 5b).

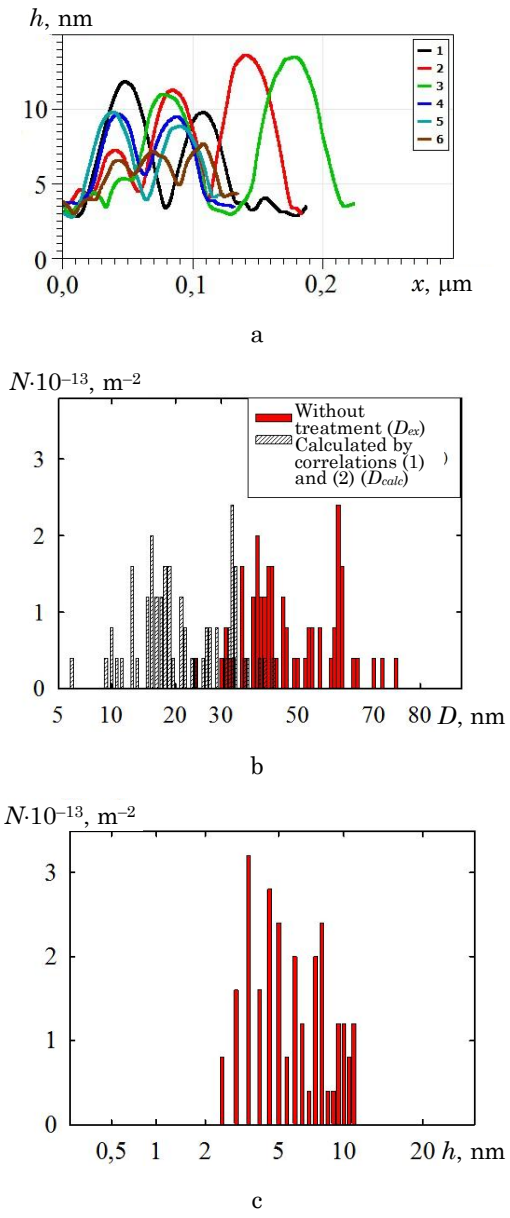

Fig. 5 – Surface profiles of the array of Ni NP on the Si_3N_4/Si substrate (a) and measured by the AFM image distributions of NP over horizontal D (b) and vertical h (c) dimensions. Dashed histogram on the position (b) shows calculated NP diameter D_{calc} at the radius of needle curvature of r = 12 nm and angle at vertex of θ = 15°

In Fig. 6 we illustrate the dependence of the value of D_{calc} on D_{ex} (a) and NP height h on the calculated D_{calc} (b). On the diagrams we present the distributions over dimensions with taking into account the radius of needle curvature r = 8-12 nm. We should note that contribution of convolution into vertical dimensions is insignificant [7], and some smoothing of the image and decrease in the relief height can occur in a general case. In spite of this, considerable difference between particle sizes in the vertical and horizontal directions is appreciable even after calculation by the models. This is, probably, connected with the fact that NP have elliptic but not spherical shape.

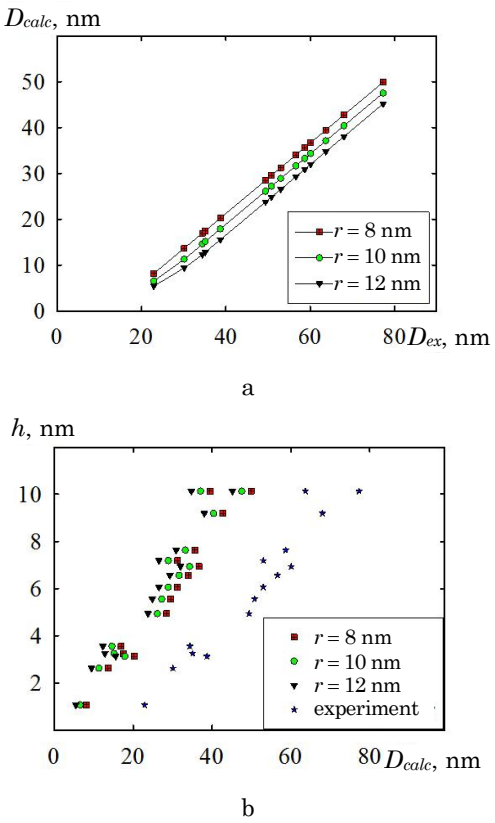

Fig. 6 – Dependence of the calculated NP diameter D_{calc} on the diameter from the AFM image D_{ex} (a) and NP height h on the calculated diameter D_{calc} (b)

As it was shown earlier in the works [1, 2, 8], morphology of the array of NP can be characterized by such parameters as the minimum D_{min}, maximum D_{max}, average D_m, and the most probable D_{prob} diameters. These parameters for the sample presented in Fig. 4 at needle radius of r = 12 nm were 2.7 nm, 21.0 nm, 10.6 nm, and 16.3 nm, respectively. The same characteristics for the height h in the vertical plane were equal to 1.5 nm, 10.5 nm, 5.4 nm, and 3.6 nm.

Similar calculations were carried out for a series of the obtained arrays of Ni and Co NP. Total data is given in Table 1. The resulting dependences of the average NP dimensions on the initial effective film thickness t were built based on the results of calculations (Fig. 7).

Dependences imply the gradual increase in the horizontal and vertical particle dimensions with the increase in the initial effective film thickness. The data given in Table 1 indicates that in a general case particle height is 2-4 times less than their diameter. In the previous work [2] we have described the investigation results of the structure and phase composition of arrays of Co NP obtained by thermal dispersion of thin metal films (the initial effective thickness of Co layer was 1.5-2.1 nm) on polyimide substrates. Morphology parameters of arrays were calculated based on the results of the transmission electron microscopy. Average NP diameter was equal to 8.8-13.0 nm. This value is slightly less than for arrays of NP on Si_3N_4/Si substrates. This can be explained by the difference in the dispersion process of thin metal layers on different substrates and different measurement accuracy of the AFM and TEM methods (since for the calculations of particle dimensions by the AFM images we have used the passport data of needle, but, as it was noted earlier, real radius of probe curvature can be larger than the passport one). However, in whole, one can conclude with high probability that NP on polyimide substrates also have elliptic shape.

Precise determination of the NP height is of a great importance, in particular, in the modeling of the behavior of their properties in an alternating magnetic field, since magnetic properties of NP strongly depend on their shape. Thus, during the transition from spherical shape to the extended one in the horizontal plane, remagnetization mechanism is changed at certain boundary values, and magnetic vortices can appear in a particle [9-11].

For the array of Co NP illustrated in Fig. 4c, d (and array with similar surface morphology, but somewhat larger D_{av}), measurements of the amplitude Ψ and phase shift Δ before and after annealing of the samples were performed by the method of spectroscopic ellipsometry. Based on the AFM data, average height of particles h_{av} is equal to 3.3 and 3.6 nm for the first and the second samples, respectively. As a result of the solution of the inverse ellipsometry problem, data about optical constants and layer thickness in systems wase obtained.

Experimental and calculated data is represented in Table 2.

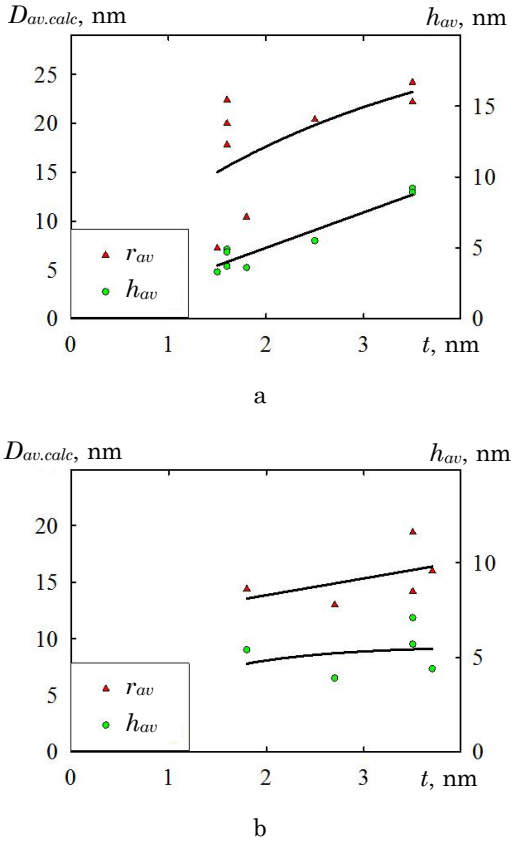

Fig. 7 – Dependence of the average calculated diameter $D_{av.calc}$ and height h of Co (a) and Ni (b) NP on the initial effective film thickness t

Table 1 – Calculation results of the real NP dimensions by correlations (1) and (2) (r = 12 nm, θ = 15°)

Material	Substrate material	Initial effective film thickness, nm	Annealing temperature, K	$D_{min.calc}$, nm	$D_{max.calc}$, nm	$D_{av.calc}$, nm	$D_{prob.calc}$, nm	h_{min}, nm	h_{max}, nm	h_{av}, nm	h_{prob}, nm
Co	Si_3N_4/Si	1.5	1020	5.2	15.6	10.4	11.4	2.8	13	7.2	9.4
Co	Si_3N_4/Si	1.5	1020	4.4	14	7.2	7.6	3.6	10.4	6.6	8
Co	Si_3N_4/Si	1.6	1050	8.2	37.4	20	16.6	2.8	24.4	9.8	7
Co	Si_3N_4/Si	1.6	1100	8.4	30.8	17.8	14.2	4	11.4	7.4	11
Co	Si_3N_4/Si	1.6	1200	6.8	36	22.4	19.6	3	17.4	9.4	13
Co	Si_3N_4/Si	2.5	1200	7.4	71.8	20.4	19.6	3	39.8	10.6	11
Co	Si_3N_4/Si	3.5	1100	8.4	108.8	24.2	19.6	4.2	114.6	18.4	17
Co	Si_3N_4/Si	3.5	1200	5.2	64.6	22.2	12	4.4	57	17.8	15
Ni	Al_2O_3	1.5	300	16.6	95.8	51.6	28.8	7.4	51	26.8	11
Ni	Si_3N_4/Si	1.5	300	7	87.2	45.6	12	4.2	56.6	22.8	8
Ni	Si_3N_4/Si	1.8	990	5.4	42	14.4	32.6	3	21	10.8	7.2
Ni	Al_2O_3	2.5	300	13.8	117.8	40	22	3	57.4	17.4	9
Ni	Si_3N_4/Si	2.5	300	11.4	124.4	42.4	25.8	2.4	61.8	17	8
Ni	Si_3N_4/Si	2.7	990	2.4	31.8	13	8.2	2.2	19.2	7.8	6
Ni	Al_2O_3	3.5	990	3.6	52.4	19.4	15.8	1.6	65	14.2	14
Ni	Si_3N_4/Si	3.5	990	2.8	51.4	14.2	9.4	3.2	45.6	11.4	7
Ni	Si_3N_4/Si	3.7	990	6	52.2	16	8.2	2.2	31.2	8.8	7

Table 2 – Optical parameters, thickness of the film system before annealing and arrays of Co NP Si_3N_4/Si substrate

Layer material	Tabulated data		Thickness of the annealed film system (quartz)	Average height of the relief by the AFM data of array of NP (after annealing)	Calculated data using GA		
	n	k	t, nm	h_{av}, nm	n	k	d, nm
Co(1.5)/Si_3N_4/Si, Δ_{ex} = – 58.771, Ψ_{ex} = 37.427							
Co	2.213	4.171	1.5	–	2.260	4.011	3.1
Si_3N_4	2.021	0	–	–	2.070	0	294.5
Si	3.874	– 0.015	–	–	4.028	– 0.014	–
Co(1.8)/Si_3N_4/Si, Δ_{ex} = – 59.754, Ψ_{ex} = 34.872							
Co	2.213	4.171	1.8	–	2.252	4.093	3.2
Si_3N_4	2.021	0	–	–	2.072	0	294.5
Si	3.874	– 0.015	–	–	4.054	–0.014	–
Co(1.5)/Si_3N_4/Si (T_{an} = 1020 K), Δ_{ex} = – 58.926, Ψ_{ex} = 37.796							
Co	2.213	4.171	1.5	3.3	2.264	4.187	3.5
Si_3N_4	2.021	0	–	–	2.071	0	294.5
Si	3.874	– 0.015	–	–	4.039	– 0.015	–
Co(1.8)/Si_3N_4/Si (T_{an} = 1020 K), Δ_{ex} = – 59.388, Ψ_{ex} = 34.735							
Co	2.213	4.171	1.8	3.6	2.293	4.218	3.7
Si_3N_4	2.021	0	–	–	2.072	0	295.1
Si	3.874	– 0.015	–	–	4.036	– 0.014	–

Calculated optical constants for Co layers before and after annealing almost coincide with the tabulated data: n = 2.272 ± 0.02 (tabulated 2.213) and k = 4.114 ± 0.104 (tabulated 4.171). Thicknesses of Co layers defined by the ellipsometry data correlate well with the AFM data. For the first sample calculated thickness of Co layer is equal to 3.51 nm (by the AFM data 3.3 nm), and for the second one – 3.66 nm (by the AFM data 3.6 nm).

4.2 Modeling of the magneto-optical properties of arrays of NP

Calculation results of the NP dimensions were tested in the modeling of their magneto-optical properties. MOKE investigations in the longitudinal measurement geometry were carried out for the arrays of Ni and Co NP with different characteristic dimensions of NP and distance between them. We should note that all arrays of NP on the MOKE dependences exhibited ferromagnetic properties. Software oommf was used for modeling of the magnetic hysteresis loops of arrays of NP [3]; Landau-Lifshitz [12] and Brown [13] correlations were used in the calculations. Models re-generated by the AFM images and re-calculated by correlations (1) and (2) were used as the calculation models. Since electron diffraction study of the phase composition of arrays of Ni and Co NP on polyimide substrates [1, 2], obtained during previous investigations, has shown that they consist of the fcc-phase; cubic anisotropy of the material was chosen for the calculations (the value of K_1 was equal to -5.7×10^3 and 2.5×10^5 J/m^3 for Ni and Co, respectively), magnetization of saturation $M_s = 450 \times 10^3$ A/m and 1200×10^3 A/m (for Ni and Co, respectively). Experimental and calculated dependences are shown in Fig. 8.

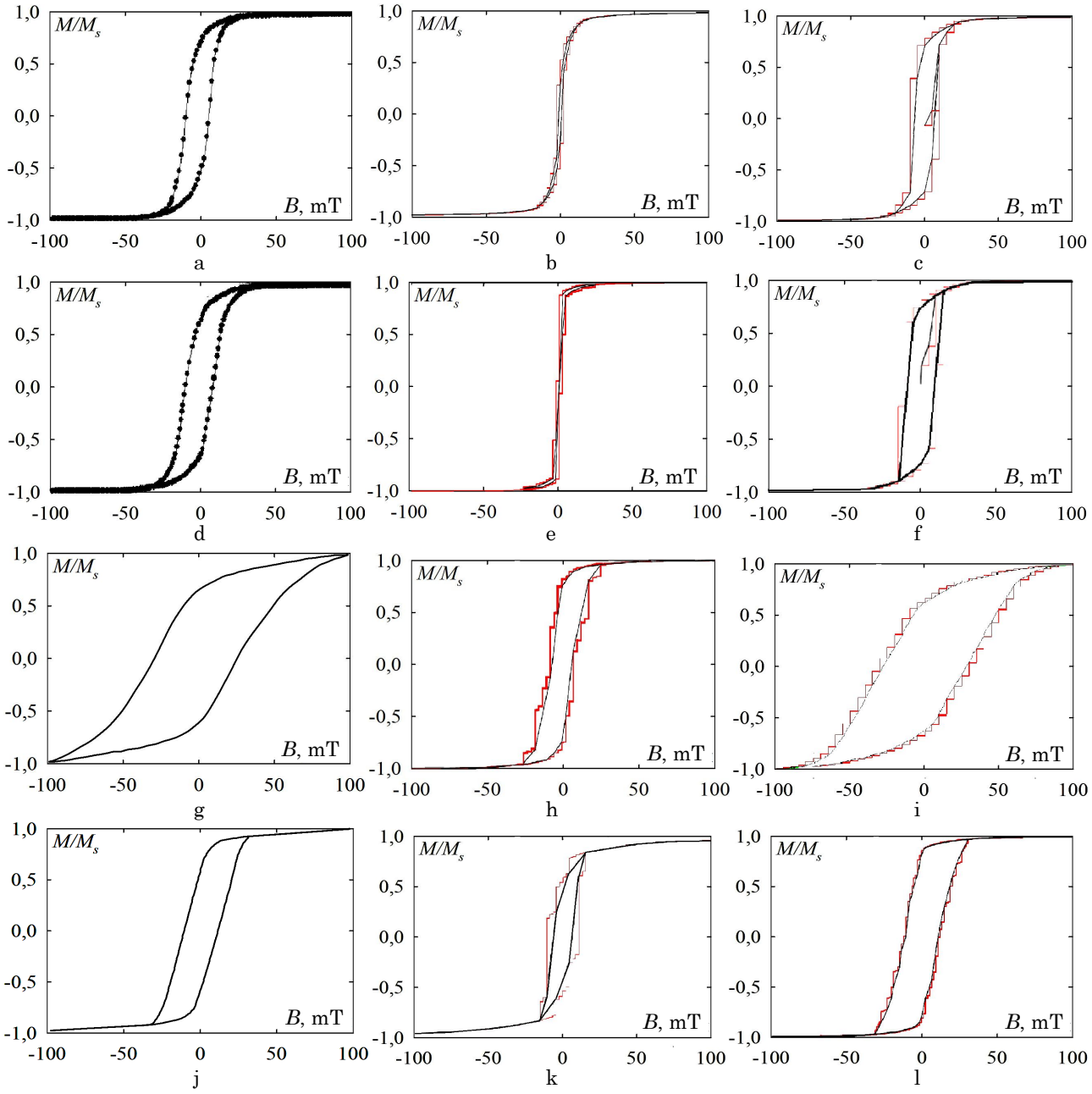

Fig. 8 – Experimental (a, d, g, j) MOKE hysteresis loops of the arrays of Ni (a, d) and Co (g, j) NP and modeled using NP dimensions without taking into account the convolution effect (b, e, h, k) and with taking into consideration the convolution effect treated by correlations (1) and (2) (c, f, i, l) models of the magnetic hysteresis loop. Average calculated NP diameter in array $D_{av.calc}$ is equal to 14.4; 16.0; 20.0 and 10.4 nm

5. CONCLUSIONS

Having compared the experimental and calculated data, one can conclude that for arrays of Ni and Co NP a good coincidence between them is only observed at the change in the geometric model of the sample with taking into account the influence of the increase in the particle dimensions on the AFM image by the phenomenon of convolution. The applied estimation technique of the real NP dimension has shown good results, and, thus, such approach in conjunction with modeling by the Landau-Lifshitz and Brown theories gives the possibility to make, in a greater degree, qualitative than quantitative prediction of the magnetic hysteresis loops of arrays of NP. Since passport data about the radius of needle curvature r and angle at its vertex θ was used during treatment of the AFM images by correlations (1) and (2), then to increase the calculation accuracy it is necessary to perform additional investigations of the geometric parameters of the AFM probe point.

REFERENCES

1. V.O. Zlenko, S.I. Protsenko, *Metallofiz. Noveishie Technol.* **33** No4, 496 (2011).
2. V.O. Zlenko, S.I. Protsenko, *Nanosystemy, nanomaterialy, nanotekhnologii* **9** No3, 607 (2011).
3. http://math.nist.gov/oommf/.
4. K.-ichi Shiramine, S. Muto, T. Shibayama, N. Sakaguclii, H. Ichinose, T. Kozaki, S. Sato, Y. Xakata, H.N. Yokoyama, M. Taniwaki, *J. Appl. Phys.* **101**, 033527 (2007).
5. S. Xu, M.F. Arnsdorf, *J. Microscopy* **187**, 43 (1997).
6. Z.-gang Zeng, G.-dong Zhu, Z. Guo, L. Zhang, X.-jian Yan, Q.-guo Du, R. Liu, *Ultramicroscopy* **108**, 975 (2008).
7. M.S. Vakstein, N.V. Aratov, V.V. Zosimov, *Molekulyarnye tekhnologii* **1**, 1 (2007).
8. V.A. Zlenko, M.G. Demydenko, S.I. Protsenko, et al., *J. Nano-Electron. Phys.* **4** No 4, 04023 (2012).
9. N.A. Usov, C.-R. Chang, Z.-H. Wei, *J. Appl. Phys.* **89**, 7591 (2001).
10. Yu.B. Grebenshchikov, N.A. Usov *J. Appl. Phys.* **93**, 4810 (2003).
11. Yu.B. Grebenshchikov, N.A. Usov, K.S. Pestchanyi, *J. Appl. Phys.* **94**, 6649 (2003).
12. L. Landau, E. Lifshitz, *Phys. Zs. d. Sowjetunion* **8** No2, 153 (1935).
13. W.F. Brown Jr., *Micromagnetics* (New York-London: Interscience Publishers: 1963).